ON THE HOT GAS CONTENT OF THE MILKY WAY HALO

Taotao Fang[1,2], James Bullock[2], and Michael Boylan-Kolchin[2,3]
(Received; Revised; Accepted)
Draft version November 6, 2012

ABSTRACT

The Milky Way appears to be missing baryons, as the observed mass in stars and gas is well below the cosmic mean. One possibility is that a substantial fraction of the Galaxy's baryons are embedded within an extended, million-degree hot halo, an idea supported indirectly by observations of warm gas clouds in the halo and gas-free dwarf spheroidal satellites. X-ray observations have established that hot gas does exist in our Galaxy beyond the local hot bubble; however, it may be distributed in a hot disk configuration. Moreover, recent investigations into the X-ray constraints have suggested that any Galactic corona must be insignificant. Here we re-examine the observational data, particularly in the X-ray and radio bands, in order to determine whether it is possible for a substantial fraction of the Galaxy's baryons to exist in $\sim 10^6$ K gas. In agreement with past studies, we find that a baryonically closed halo is clearly ruled out if one assumes that the hot corona is distributed with a cuspy NFW profile. However, if the hot corona of the galaxy is in an extended, low-density distribution with a large central core, as expected for an adiabatic gas in hydrostatic equilibrium, then it may contain up to 10^{11} M$_\odot$ of material, possibly accounting for all of the missing Galactic baryons. We briefly discuss some potential avenues for discriminating between a massive, extended hot halo and a local hot disk.

Subject headings: Galaxy: halo — X-rays: diffuse background

1. INTRODUCTION

The question of whether or not significant reservoirs of hot baryons exist around bright field galaxies remains a topic of current debate (Dai et al. 2010; Anderson & Bregman 2010; Humphrey et al. 2011; Prochaska et al. 2011) despite years of discussion in the literature (Spitzer 1956; Bahcall & Spitzer 1969; Mo & Miralda-Escude 1996; Mo & Mao 2002). Theoretical prejudice favors the idea that quasi-stable $\sim 10^6$ K coronae develop as shock-heated material in the aftermath of halo collapse (Silk 1977; White & Rees 1978; White & Frenk 1991; Benson et al. 2000; Kereš et al. 2005; Dekel & Birnboim 2006; Kereš & Hernquist 2009; Crain et al. 2010), though the density structure and mass content of these halos is sensitive to uncertain physics and energy injection processes (White & Rees 1978; Maller & Bullock 2004; Kaufmann et al. 2009; Benson 2010; Sharma et al. 2012).

If hot gaseous halos exist, they would provide a potential hiding place for *missing galactic baryons* – the $\gtrsim 80\%$ of baryons that are unaccounted for by collapsed gas and stars in galaxies (e.g., Fukugita et al. 1998; Anderson & Bregman 2010; Behroozi et al. 2010; Moster et al. 2012). It is not known whether the missing halo baryons exist primarily as diffuse hot gas halos around normal galaxies (Maller & Bullock 2004; Fukugita & Peebles 2006; Sommer-Larsen 2006), have been mostly expelled as a result of energetic blow out (Dekel & Silk 1986; Almeida et al. 2008), or were never accreted in the first place, possibly as a result of pre-heating (e.g. Mo et al. 2005). So far, searches have failed to detect extended X-ray emission around nearby spiral galaxies (e.g., Bregman et al.

1998; Benson et al. 2000; Rasmussen et al. 2009). Most of the detected X-ray emission in these galaxies is centered around disk/bulge region, and is associated with active star formation regions (see, e.g., Wang 2007; Li et al. 2007).

Locally, the Milky Way provides an important benchmark for understanding the missing galactic baryon problem. The Galaxy's dark matter halo mass is somewhat uncertain, but maser observations, stellar halo tracers, and satellite kinematics suggest a total virial mass[4] in the range $M_v = (1-2) \times 10^{12}$ M$_\odot$ (see Boylan-Kolchin et al. 2012 for a summary), within an associated virial radius $R_v \simeq (260-330)$ kpc. In the absence of mass loss, the Milky Way's baryonic allotment therefore should be $M_b = f_b\,M_v \simeq (1.65-3.3)\times10^{11}$ M$_\odot$, assuming a universal baryon fraction $f_b = 0.165$ (consistent with Komatsu et al. 2011). The observed cold baryonic mass of the Milky Way is well below this, $M_\star \simeq 0.65 \times 10^{11}$ McMillan & Binney (2012), with effectively negligible contributions from cool disk gas (Kalberla & Kerp 2009) and satellite galaxies (McConnachie 2012). At least 10^{11} M$_\odot$ of baryons are missing from the Galactic census.

There is circumstantial evidence that at least some of these missing Galactic baryons are in an extended, hot corona. For example, a confining hot medium can help explain gas clouds in the Magellanic Stream (Stanimirović et al. 2002), and the shapes of shells along the edge of the Large Magellanic Cloud (de Boer et al. 1998) are similarly suggestive. H-alpha emission at the leading edge of the Magellanic stream is best understood via heating from a fairly dense hot medium ($\sim 10^{-4}$ cm^{-3} at ~ 50 kpc; Weiner & Williams 1996). The thermal pressure of high-velocity clouds at the same distance is

[1] Department of Astronomy and Institute of Theoretical Physics and Astrophysics, Xiamen University, Xiamen, Fujian 361005, China
[2] Department of Physics & Astronomy, 4129 Frederick Reines Hall, University of California, Irvine, CA 92697
[3] Center for Galaxy Evolution Fellow

[4] We define the virial mass using an average enclosed density of $\Delta = 95$ times the critical density of the Universe, as determined using the spherical top-hat collapse model in the LCDM cosmology.

consistent with a similar confining medium (Fox et al. 2005). More recent ultraviolet and optical absorption probes of the Magellanic Stream provide strong evidence for a complex, multi-phase structure that is being evaporated by interactions with a hot corona (Fox et al. 2010). The head-tail structure of high velocity clouds is another observation best explained in the context of a confining corona (Putman et al. 2011). A separate argument for the existence of such a medium is the lack of detected HI in most dwarf spheroidal galaxies within 270 kpc of the Milky Way (Grcevich & Putman 2009) – a result that is naturally explained by ram pressure stripping by a $\sim 10^{-4}$ cm^{-3} hot medium at ~ 70 kpc (see also Moore & Davis 1994; Lin & Faber 1983; Nichols et al. 2011).

While these indirect probes are enlightening, the most direct avenue for detecting a hot corona is via X-ray studies. It is well known that the soft X-ray background (between 0.1 and 2 keV) consists of three components: the Local Hot Bubble (LHB), extragalactic emission (mostly from active galactic nuclei), and a thermal component that lies at an intermediate distance (see, e.g., Kuntz & Snowden 2000). One popular interpretation of this thermal component is that it originates from the hot interstellar medium (ISM) in the Galactic disk, i.e., a hot gas disk rather than a ~ 100 kpc extended Galactic halo. Indeed, using joint X-ray emission-absorption analysis, Yao et al. (2009a) and Hagihara et al. (2010) argued that the hot gas in our Galaxy is confined within a few kpc around the stellar disk. The detection of the highly ionized metal absorption lines at $z = 0$ in numerous quasar spectra also suggested a hot gas component in and around our Galaxy (see, e.g., Nicastro et al. 2002; Fang et al. 2003, 2006; Bregman & Lloyd-Davies 2007; Gupta et al. 2012); however, it is also unclear this absorption is produced by hot gas in the disk or distant halo. Anderson & Bregman (2010) focused specifically on the question of baryonic closure, asking whether the dispersion measure of pulsars in the Large Magellanic Cloud (LMC) could be reconciled with a baryonically closed Milky Way halo. They concluded that it could not, though they focused mainly on cases where the hot gas follows a cuspy density profile characterized by either a single power law or a broken power law (as expected for dissipationless dark matter).

In what follows, we re-examine the question of the the Milky Way's hot corona in the context of X-ray surface brightness constraints and pulsar dispersion measurements from the standpoint of three illustrative models for the hot gas density distribution: (1) an extended profile with a central core, as expected for an adiabatic gas in hydrostatic equilibrium (Maller & Bullock 2004, hereafter MB); (2) a centrally concentrated Navarro, Frenk, & White (1997, NFW) profile and (3) a local hot gas disk. The first profile is among the puffiest distributions one might consider, though it is in fact very similar to predictions for realistic galaxy-size halos with gaseous halos that are in both hydrostatic and thermal equilibrium (Sharma et al. 2012). The second profile we consider, the NFW hot halo, is the most centrally concentrated distribution that one could envision for a hot gas around a galaxy, given that it is the profile that arises from the collapse of non-interacting dust. While it is unclear how such a profile could arise in a real astrophysical plasma, this is an assumption that often appears in the literature.

The third case explores a scenario where all of the X-ray gas detections are explained by a local distribution with globally negligible mass content ($< 10^8$ M$_\odot$).

2. MODEL DEFINITIONS

In our fiducial explorations, we assume that the Milky Way's dark matter halo has a virial mass of $M_v = 10^{12}$M$_\odot$ (with associated radius $R_v = 260$ kpc) and that it follows an NFW profile with a concentration of $C_v = 12$ (and thus a scale radius $R_s = 21.7$ kpc; Navarro et al. 1997; Bullock et al. 2001). The implied mass in missing baryons is approximately 10^{11}M$_\odot$. We then explore the three aforementioned hot gas distributions, including two coronal models that contain $M_{hot} = 10^{11}$ M$_\odot$ of material, in this context.

2.1. *Extended Adiabatic Halo: MB*

The first model we explore, MB, assumes that the hot halo is distributed as adiabatic gas with polytropic index of 5/3 that is in hydrostatic equilibrium within the Milky Way's NFW dark matter halo of concentration C_v (Maller & Bullock 2004):

$$\rho_g^{MB}(r) = \rho_v \left[1 + \frac{3.7}{x} \ln(1+x) - \frac{3.7}{C_v} \ln(1+C_v) \right]^{3/2},$$
(1)

where r is the radius from the Galactic center and $x \equiv r/R_s$, with R_s the scale radius of the dark matter halo. The density ρ_v is the gas density at the virial radius. In our fiducial case, we chose ρ_v such that the integrated hot gas mass within R_v is $M_{hot} = 10^{11}$M$_\odot$. The resulting temperature profile is

$$T_g^{MB}(r) = T_v \left[1 + \frac{3.7}{x} \ln(1+x) - \frac{3.7}{C_v} \ln(1+C_v) \right],$$
(2)

where T_v is the hot halo temperature at R_v. We set T_v by requiring that the X-ray emission-weighted temperature be consistent with *XMM*-Newton and *Suzaku* observations, which both give halo temperatures consistent with $T_h = 0.2$ keV, with errors of $\sim 10\%$. The normalization, T_v, is then determined by:

$$T_h = \frac{\int \rho^2(r) \Lambda(T, Z_g) T(r) dr}{\int \rho^2(r) \Lambda(T, Z_g) dr},$$
(3)

where $\Lambda(T, Z_g)$ is the cooling function (Sutherland & Dopita 1993) and we assume a $Z_g = 0.3 Z_\odot$ (results for different choices of Z_g are explored in Section 4.1). The implied density, temperature, pressure, and mass profiles for the MB model are shown as solid black lines in Figure 1.

2.2. *Cuspy Halo: NFW*

As mentioned in the introduction, it is common to make the simplifying assumption that the density distribution of the hot gas around galaxies traces what is expected for the dark matter alone:

$$\rho_g^{NFW}(r) = \frac{\rho_g}{x(1+x)^2}.$$
(4)

As before, $x \equiv r/R_s$, where $R_s \equiv R_v/C_h$ is the NFW scale radius. We explicitly allow C_h to be different than
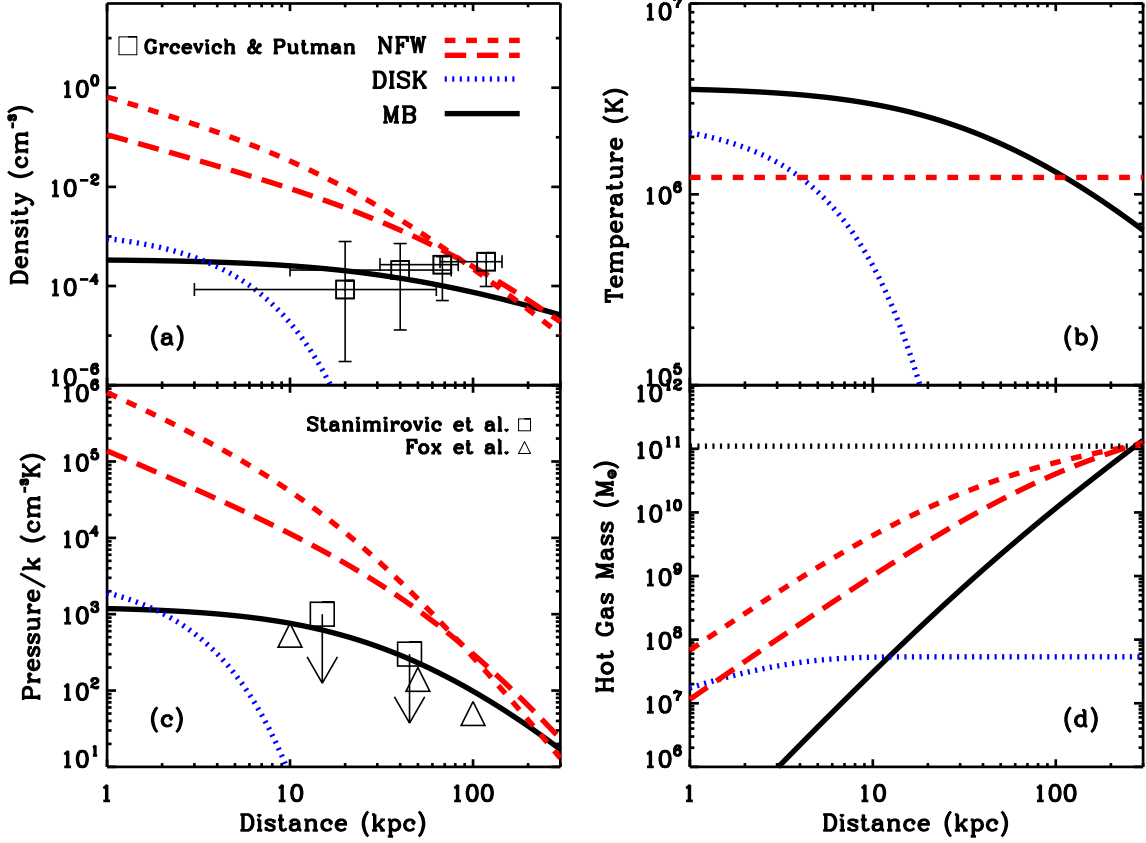
FIG. 1.— Hot gas profiles as a function of radius. *Panel (a)*: density; *panel (b)*: temperature; *panel (c)*: pressure; *panel (d)*: hot gas mass. The predictions from the MB model are plotted in solid black, the DISK model in dotted blue, and NFW models with $C_v = 12$ (3) in red dash (dot-dash). For the DISK model, the x-axis is actually the vertical distance (z) from the disk. The square symbols in panel (a) show estimates of the hot gas density required to explain the lack of HI in Milky Way dwarf galaxies as derived from ram pressure striping arguments by Grcevich & Putman (2009). The square symbols in panel (c) are derived by Stanimirović et al. (2002) and Fox et al. (2005) under the assumption that high velocity clouds in the Milky Way halo are pressure-confined. See text for details.

C_v of the background dark matter halo. As before, we fix the normalization ρ_g by requiring that the total hot gas mass within the virial radius equals $10^{11} M_\odot$. For the NFW profile, we assume a constant hot halo temperature of T_h. This requires an unusual equation of state profile that varies with radius for self-consistency, but we adopt it here for comparison to previous work.

We explore two cases for the NFW hot halo concentration: $C_h = 12$ (which mimics the dark matter background exactly: $C_h = C_v$) and also a low-concentration case with $C_h = 3$. The implied density, temperature, pressure, and mass profiles for the high (low) concentration NFW case are shown by the dashed (dot-dashed) lines in Figure 1.

2.3. *Local Model: DISK*

For comparison, we also calculate the hot gas distribution in an exponential disk model, which has been favored by recent X-ray observations. Following Yao et al.

(2009b), we adopt a vertical distribution

$$\rho_g^{\mathrm{DISK}}(z) = \rho_0 \exp\left(-\frac{z}{h_\rho \xi}\right), \quad (5)$$

and

$$T_g^{\mathrm{DISK}}(z) = T_0 \exp\left(-\frac{z}{h_T \xi}\right), \quad (6)$$

Here ξ is the volume filling factor and is assumed to be 1, z is the vertical distance from the disk, ρ_0 and T_0 are the gas density and temperature at the disk mid-plane, and h_ρ and h_T are the scale height of the hot gas density and temperature distributions, respectively.

We set $\rho_0 = 1.4 \times 10^{-3}$ cm^{-3}, $h_\rho = 2.3$ kpc, $T_0 = 10^{6.4}$K, and $h_T = 5.6$ kpc based on observations of the PKS 2155-304 sight line (Hagihara et al. 2010). Yao et al. (2009a) observed the LMC X-3 sight line and reached similar conclusion. This model is plotted in blue in Fig-

ure 1; the y-axis is the vertical distance from the Galactic disk ($|z|$) since in the model the density and temperature depends only on this distance.

3. OBSERVATIONAL CONSTRAINTS

3.1. *Indirect Probes*

One of the strongest pieces of indirect evidence for an extended hot gas reservoir around the Galaxy comes from the lack of gas detected in small dwarf satellite galaxies around the Milky Way. Dwarf galaxies tend to be gas rich unless they are within close (~ 300 kpc) proximity of a larger system, an observation that is usually interpreted as arising from ram-pressure stripping Lin & Faber 1983; Moore & Davis 1994.

Recently, Grcevich & Putman (2009) examined the HI content of the Local Group dwarf galaxies. They found a cut-off radius of ~ 270 kpc around the Milky Way or Andromeda, below which no dwarf spheroidal galaxy contains detected HI gas. They argued the ram-pressure stripping produced by a hot, extended halo gas can explain the lack of the HI gas in these dwarfs, and they constrained this gas density by the measurements of four dwarfs, Carina, Ursa Minor, Sculptor, and Fornax, between ~ 20 to 100 kpc. The data points and their error bars are plotted in the top left panel of Figure 1. These measurements are much too extended to be explained by a local disk model (blue dotted) and too low density to be explained by the cuspy NFW models (red); they are matched reasonably well by the MB distribution, however.

A completely distinct indication for extended hot gas comes from studying gas clouds around the galaxy. Relying on the Arecibo telescope, Stanimirović et al. (2002) observed the Magellanic Stream in HI 21-cm emission. They found that the most likely mechanism to confine the stream clouds is via pressure from a hot halo. They placed upper limits on the hot gas pressure at 10^3 and 3×10^{-2} cm^{-3}K at 15 and 45 kpc, respectively (square symbols in Figure 1, bottom left panel). Fox et al. (2005) have reached similar conclusions when studying high velocity clouds (HVCs) in the halo. These authors concluded that if HVCs are pressure-confined, then the pressure of the surrounding medium must be approximately 530, 140, and 50 cm^{-3}K, at distances of 10, 50, and 100 kpc, respectively (triangles in Figure 1, bottom left panel). Again, while neither the NFW nor DISK models matches these constraints, the extended MB model provides pressure support at approximately the required level.

Of course, neither the cloud-confinement arguments nor the ram-pressure stripping arguments individually demands the existence of an extended hot halo. It may be possible that some other environmental process can explain the lack of gas in local dwarfs, though there is no obvious candidate for such a mechanism. Similarly, it is possible that warm gas clouds in the Galactic halo are not pressure-confined. The confinement could, in principle, be gravitational if the clouds are embedded within dark matter halos (Sternberg et al. 2002). Nevertheless, it is interesting to recognize that an extended hot gas halo containing a substantial fraction of the halo's baryons is capable of matching both constraints quite well.

3.2. *X-ray Emission*

X-ray emission provides a strong constraint on the extent and density of hot gas around the Galaxy. We consider data from two recent surveys with the *XMM-Newton* and *Suzaku* X-ray telescopes. Henley & Shelton (2010) studied 26 high-latitude *XMM*-Newton observations of diffuse X-ray emission ($|b| > 30°$ where b is the Galactic latitude). The Galactic longitudes (l) of these observations were selected to be between $120°$ and $240°$ to avoid enhanced emission from the Galactic center. Yoshino et al. (2009) studied the soft, diffuse X-ray emission in 12 fields observed with the *Suzaku* X-ray Telescope. The Galactic longitudes and latitudes are similar to those *XMM* fields, i.e., high latitudes and away from the direction of the Galactic center, except two fields at $b = 10°$ and $20°$.

While the exact details differ between the two analyses, the general procedures are similar (see their papers for details). After cleaning the spectrum, they fitted the observed spectrum to three components: (1) the cosmic X-ray background; (2) local thermal plasma emission at a temperature around 0.1 keV from solar wind charge exchange (SWCX) and local hot bubble (LHB) emission; and (3) distant thermal emission from near the Galaxy but beyond the LHB. The third component is the one that we consider here as likely arising from the distant halo.

In the XMM data analysis, a single power law was adopted to model the cosmic X-ray background, so we use the results presented in Table 2 of Henley et al. For the *Suzaku* data, various models for the Cosmic X-ray background were tried and we present the the one that relied on a single power law (Yoshino et al.'s Table 4) in order to directly compare with the XMM result. We select the energy band between 0.4 and 2 keV (the default value adopted in the XMM data analysis) to compare the observed and modeled X-ray surface brightness ($S_X^{\rm OBS}$). Since for the *Suzaku* data $S_X^{\rm OBS}$ were not calculated, we estimate the $S_X^{\rm OBS}$ using their models with the software package XSPEC; specifically, we use their model 1' (see their Table 4), which adopted a power law model of the CXB. The resultant normalized data is plotted in the left panel of Figure 2. The grey area indicates the full range of the data, which we will use as a benchmark comparison for our model predictions.

We make predictions for the X-ray surface brightness from each of our hot gas models using

$$S_X = \frac{1}{4\pi} \int \rho_e(r)\rho_i(r)\Lambda[T(r)]dr. \qquad (7)$$

Here ρ_e and ρ_i are the electron and proton densities, and $\Lambda(T)$ is the cooling function. In order to compare with observations, we use the Astrophysical Plasma Emission Code (APEC)[5] to calculate the X-ray emissivity between 0.4 and 2 keV as a function of plasma temperature. Since the X-ray emissivity is also a function of metal abundance, we assume a $Z_g = 0.3Z_\odot$ for the MB and NFW models (Cen & Ostriker 2006; Rasmussen & Ponman 2009), and $1 Z_\odot$ for the DISK model, where $Z_\odot$ is the solar abundance of Anders & Grevesse (1989). We explore the effect of these choices on our predictions below.
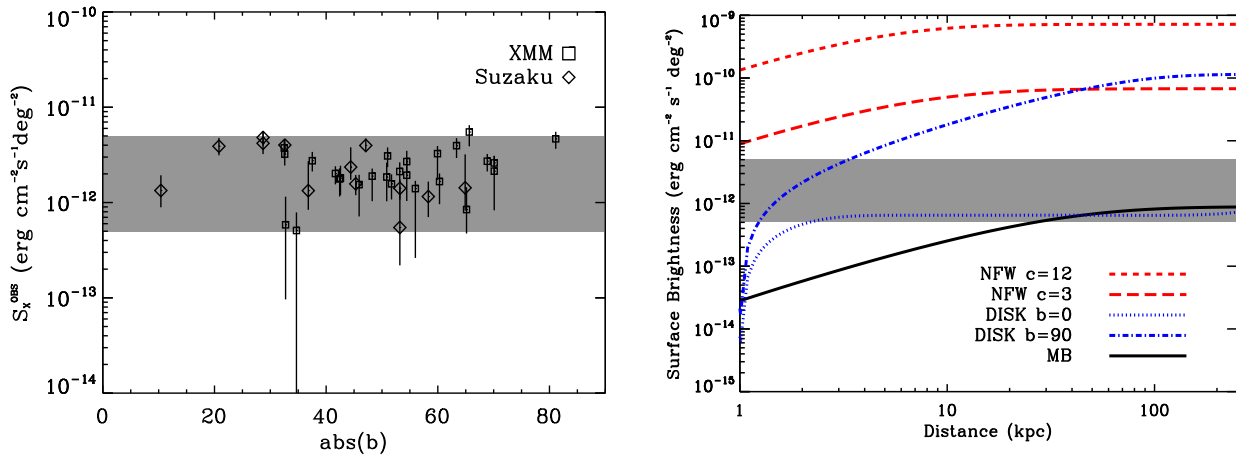
---

[5] See http://atomdb.org/.

FIG. 2.— X-ray emission constraints. *Left panel*: X-ray surface brightness between 0.4 and 2 keV as a function of Galactic latitude. *XMM* data are shown as squares, and *Suzaku* as diamonds (see text for details). The grey region shows the range of variation. *Right panel*: Model predictions of the X-ray surface brightness between 0.4 and 2 keV as a function of radius. Lines are the same as shown in Figure 1; however, we plot the DISK model prediction for two b values, 0° (upper blue dotted curve) and 90° (lower blue dotted curve). The grey area is reproduced from the left panel.

In the right panel of Figure 2, we plot the predicted surface brightness for our three models as the integrated emission coming from gas within a given distance (horizontal axis). The grey band is the constraint from observations – the upper limits of the X-ray emission from the hot diffuse gas. Note that even though both *XMM*-Newton and *Suzaku* observations avoid the X-ray bright sky toward the Galactic center, we expect some sightlines may still experience local enhancement from supernova heating.

Figure 2 clearly indicates the NFW profiles predict far too much X-ray emission. In particular, the $C_v = 12$ case exceeds observations by more than two orders of magnitude. This is consistent with the results of Anderson & Bregman (2010), and it comes about because the density at the center of the NFW profile is far too high (see the left panel of Figure 1). Indeed, the $C_v = 3$ profile also substantially over-predicts the X-ray emission. We see from the rise of the line with distance that the majority of the X-ray emission comes from the inner ~ 10 kpc for both of the NFW models (red lines). Since the $C_h = 12$ hot gas NFW model is ruled out to an extreme degree, we will only include the $C_h = 3$ (low concentration) NFW halo in our comparisons for the remainder of this paper.

In contrast to the NFW model, the MB profile (solid black) is fully consistent with the data, comfortably reaching the lower part of the observed region at ~ 25 kpc. Recall that the MB profile has the same mass in hot baryons within R_v as the NFW models, so the spatial distribution of the gas obviously plays a crucial role in determining the X-ray properties of the halo. The two dotted blue curves in Figure 2 represent the the DISK model predictions for in-plane ($b = 0°$; upper curve) and vertical ($b = 90°$; lower curve) sight lines. The DISK model can also fit the observed value quite well at high Galactic latitude; however, at low Galactic latitude, it also predicts too much X-ray emission. This is partially a limitation of the simplified disk model assumed, which does not truncate in the radial plane. Unfortunately, with the current data we cannot tell whether there is a

increasing trend at low b (see the right panel of Figure 1); however, future targeted observations at low b may help distinguish between an extended hot halo like MB and a local hot distribution like the DISK model.

3.3. *Pulsar Dispersion Measure*

The dispersion measure (DM) of pulsars offers a direct probe of the electron distribution along the sight line towards a background pulsar at a distance D from the Earth:

$$\text{DM} = \int_0^D \rho_e(r)dr. \tag{8}$$

While most known pulsars live in the Milky Way disk, several have been discovered in the Large and Small Magellanic Clouds (LMC and SMC), with a distance $D \sim 50$ and 60 kpc, respectively.

Two recent surveys of pulsars in the LMC and SMC were performed by Crawford et al. (2001) and Manchester et al. (2006). They found a total of 21 pulsars, among which we selected 18 pulsars. Five of the selected pulsars are located in the SMC and the rest in the LMC. We discarded 3 pulsars with a $\text{DM} \sin |b| < 25$ cm^{-3} pc since the distribution of $\text{DM} \sin |b|$ of the Galactic pulsars suggests those pulsars likely lie within the Milky Way disk (Crawford et al. 2001; Gaensler et al. 2008). We plot the DM of the remaining pulsars – which should be associated with the Magellanic Clouds – and their errors in Figure 3. For visual clarity, we randomly assign distances between 50 and 60 kpc for these pulsars. The pulsar DMs in LMC and SMC range from 40 to ~ 200 cm^{-3} pc. Higher DMs for some of the pulsars indicate most likely a significant contribution from electrons in the LMC or SMC, so the lowest DM will provide an upper limit on the hot gas distributed between us and the LMC and SMC.

There are two important potential sources for electrons giving rise to the DM. The first is the hot gas corona, which we will explore below. The second is the warm ionized medium (WIM) in and near the disk. It has long
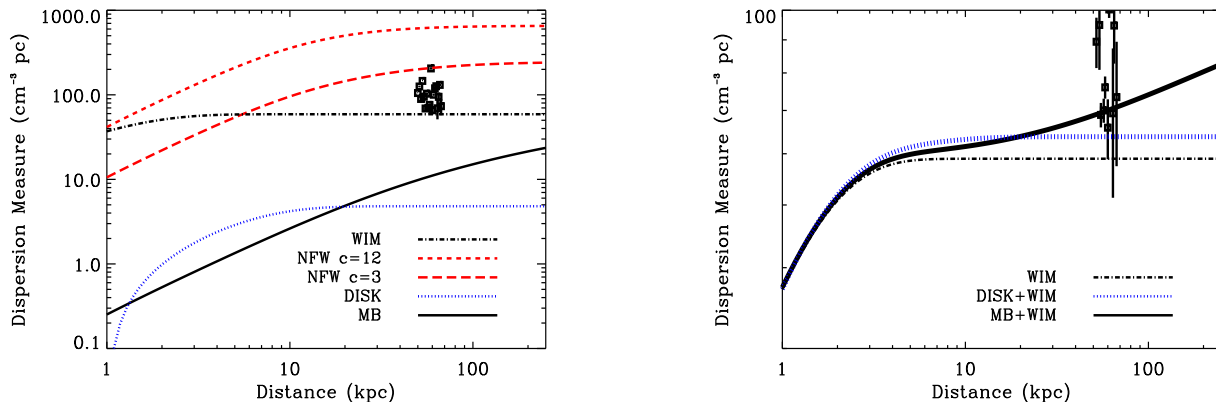
FIG. 3.— *Left panel*: Pulsar dispersion measure as a function of distance. The dash-dotted line shows the contribution from the Warm Ionized Medium (WIM) in and near the disk using the parameterization of Gaensler et al. (2008). Otherwise the MB, NFW ($C_v = 3$), and DISK line styles are the same as in Figure 1. Only the corona distributed like an NFW provides a contribution larger than the WIM and is clearly ruled out by these data. *Right panel*: We also plot the total DM from the DISK and MB models (see the thick blue and dark curves, respectively).

been suggested that the distribution of the free electrons in the WIM of the disk follows a planar distribution (see, e.g., (Reynolds 1989)):

$$n^{\text{WIM}}(z) = n_0^{\text{WIM}} \exp\left(-\frac{z}{H_n^{\text{WIM}}}\right). \qquad (9)$$

Here n_0^{WIM} and H_n^{WIM} are the mid-plane WIM electron density and the scale height, respectively. By fitting a total of 53 sightlines, Gaensler et al. (2008) found $n_0^{\text{WIM}} = 0.031^{+0.004}_{-0.002}$ cm^{-3} and $H_n^{\text{WIM}} = 1010^{+40}_{-170}$ pc; we adopt these values here. The dash-dotted line in Figure 3 shows the contribution of this WIM distribution to the DM measure. We specifically calculate the contribution along the line of sight toward the LMC. We see that it is significant, leaving very little room for additional electrons from a hot halo.

The solid black, dashed red, and dotted blue lines in the left panel of Figure 3 show the DM coming from our MB, NFW ($C_h = 3$), and DISK models, respectively. In each case we calculate the DM within a line-of-sight distance D pointed in the direction (l, b) via $D^2 = r^2 + D_0^2 - 2rD_0 \cos l \cos b$, where $D_0 = 8$ kpc is the distance between the Sun and the Galactic Center and r is the Galactocentric distance. It is clear that both the MB and DISK models produce DM contributions that are well below the WIM, such that the total WIM+DM or WIM+DISK results are consistent with the data. The $C_h = 3$ NFW model, on the other hand, is clearly inconsistent, especially when the total WIM+NFW contribution is considered.

Interestingly, the DM from the MB profile continues to rise to large radii. In principle, if we were confident about the contribution from the WIM, a dispersion measure from more distant pulsars would provide interesting constraints such an extended profile. In the right panel of Figure 3 we show the detailed difference between the total DM of the MB+WIM model (black, solid line) and the DISK+WIM model (blue, dotted line). The two models already predict significant difference at a distance

of ~100 kpc. The next brightest distant satellite (after the SMC and LMC) is the Fornax dwarf at a distance of ~ 150 kpc. To our knowledge, there are no known pulsars in Fornax (McLaughlin & Cordes 2003), but further searches would be useful.

4. DISCUSSION

4.1. *Extended Halo: Parameter Dependence*

We have demonstrated that if one considers a hot halo profile with a low density (high entropy) core, as expected for an adiabatic gas in hydrostatic equilibrium (Maller & Bullock 2004) or for a galaxy-size hot halo in hydrostatic and thermal equilibrium (Sharma et al. 2012), then the Milky Way could in principle contain the universal baryon fraction within its virial radius. Specifically, in our fiducial MB model we considered a Milky Way halo of virial mass $M_v = 10^{12}$ M$_\odot$ and a hot halo of mass $M_{\text{hot}} = 10^{11}$ M$_\odot$, which would make the system baryonically closed. The X-ray surface brightness is quite sensitive to the chosen value of the metallicity of the gas; we have so far used $Z_g = 0.3 Z_\odot$. In this section, we investigate how our MB halo results depend on our specific choice of virial mass, metallicity, and hot gas mass.

The red dashed lines in the left panel of Figure 4 show the density (top panel) and pressure (bottom panel) profiles under the assumption that the Milky Way virial mass is at the upper end of the expected range, $M_v = 2 \times 10^{12}$ M$_\odot$, and that the system is baryonically closed ($M_{\text{hot}} = 2.7 \times 10^{11}$ M$_\odot$). Note that while the density itself appears to be consistent with the Grcevich & Putman determination from HI gas stripping, the implied pressure profile is too high to explain the properties of gas clouds in the halo. The solid black lines show our fiducial model for reference and the blue, long-dashed lines show a similar halo that contains only ~ 2/3 of its baryons in total, with a hot halo mass of $M_{\text{hot}} = 5 \times 10^{10}$ M$_\odot$. This halo is fairly consistent with the Fox et al. pressure estimates, but it somewhat too low in density to explain the lack of HI in Milky Way dwarfs.
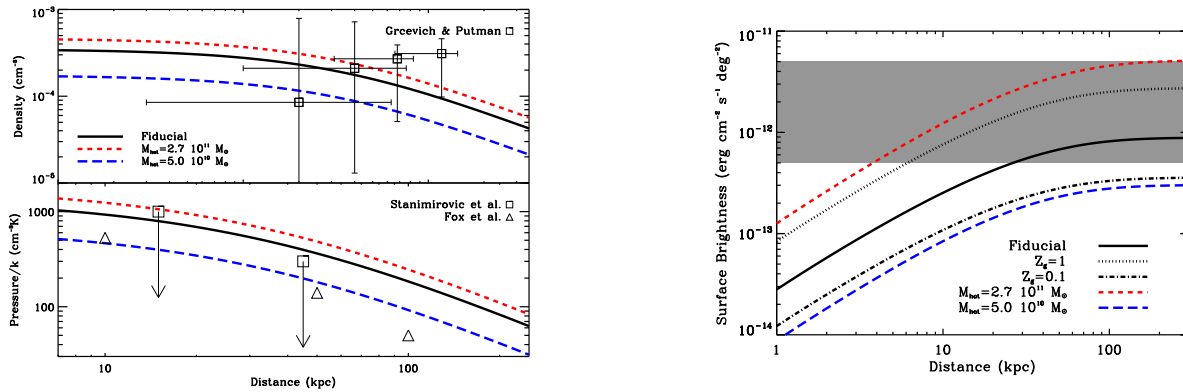
FIG. 4.— *Left panel*: Density (top) and pressure (bottom) distributions for MB profiles with $M_{hot} = 2.7$ (red dashed), 1.0 (solid black, fiducial), and 0.5×10^{11} $M_\odot$ (blue, long-dashed). *Right panel*: The X-ray surface brightness profiles for the same three models are shown with the same line types as in the left panel. In addition, the dotted and dot-dashed lines show our fiducial halo with both higher metallicity ($Z_g = 1 Z_\odot$, top) and lower metallicity ($0.1 Z_\odot$, bottom), respectively.

The same group of models are presented in the right panel in comparison to the X-ray surface brightness constraints for our fiducial metallicity assumption $Z_g = 0.3$. They are all consistent with these data. The predicted S_X values are also sensitive to metallicity, as metals increase the cooling efficiency. To investigate the effect of metals, we calculate S_X for two additional metallicities within our fiducial MB halo: $Z_g = 1 Z_\odot$ (the dotted dark line in Figure 4), and $Z_g = 0.1 Z_\odot$ (the dashed dark line). Although the predicted S_X is still consistent with observations for $Z_g = 1 Z_\odot$, it is on the high end of the observed S_X.

5. SUMMARY

Whether or not galaxies like the Milky Way host substantial masses of baryons in hot coronae has a fundamental impact on our understanding of galaxy formation and evolution. In this paper, we examined the latest X-ray emission and pulsar dispersion measure data to test for the presence of hot baryons in the distant halo of our Milky Way. The three models that we used to describe the hot gas distribution in the halo are: (1) a NFW-type; (2) an extended hot halo motivated by MB04; and (3) a disk distribution.

We found that for a baryonically closed Milky Way, the hot gas cannot follow an NFW profile, either for a standard halo concentration ($C_h = 12$) or for a low concentration ($C_h = 3$): the NFW profile predicts both too much X-ray emission and a pulsar dispersion measure that exceeds the latest observational data. The baryon fraction in such models must be substantially lower ($f_b \sim 0.01 - 0.02$) to be consistent with data (see also Anderson & Bregman 2010).

The other two classes of models we have considered – extended halos of hot gas in hydrostatic equilibrium (Maller & Bullock 2004) and a hot disk of gas – can both be made consistent with existing X-ray emission and pulsar dispersion measure data. These two models predict very different properties for the hot gas content of the Milky Way, however: in the DISK model, the hot gas contributes a negligible amount ($\sim 10^8 M_\odot$) to the Milky Way's baryon budget, while the MB extended halo model can contain enough hot gas to make the Milky Way baryonically closed.

As we were completing this work, Gupta et al. (2012) presented a complementary study of the hot gas content of the Milky Way halo using X-ray spectra of background AGNs. Based on the detected z = 0 absorption lines produced by highly ionized oxygen, O VII and O VIII, and a joint analysis with the Galactic halo emission, Gupta et al. argued for the existence of an extended hot gas around our Galaxy, with a radius of over 100 kpc and a total mass in excess of $10^{10} M_\odot$. Their conclusion is fully consistent with our results for extended hot gas profiles, and incorporating X-ray absorption data, along with considerations of uncertainties associated with the gas metallicity and ionization mechanism(s), would likely be a fruitful avenue for future extensions of our current work.

Incorporating additional indirect constraints – i.e., the lack of gas in *all* Milky Way dwarf spheroidals and the possibility that high velocity clouds are pressure-confined by a hot ambient medium – may indicate that a MB-type model with an extended hot halo is favored. This interpretation should be testable in the near future, as observations of X-ray emission at low latitudes ($|b| < 20°$) can distinguish between the MB and the DISK models. Such observations ideally should be performed at $90 < l < 270°$ to avoid the contamination from the Galactic center. If pulsars can be detected in distant dwarf spheroidal galaxies with recent star formation – e.g., Fornax and Leo I – dispersion measures for these objects would also be very constraining for the distribution of hot gas around the Milky Way.

REFERENCES

Almeida, C., Baugh, C. M., Wake, D. A., et al. 2008, MNRAS, 386, 2145

Anders, E., & Grevesse, N. 1989, Geochim. Cosmochim. Acta, 53, 197

Anderson, M. E., & Bregman, J. N. 2010, ApJ, 714, 320

Bahcall, J. N., & Spitzer, Jr., L. 1969, ApJ, 156, L63

Behroozi, P. S., Conroy, C., & Wechsler, R. H. 2010, ApJ, 717, 379

Benson, A. J. 2010, Phys. Rep., 495, 33

Benson, A. J., Bower, R. G., Frenk, C. S., & White, S. D. M. 2000, MNRAS, 314, 557

Boylan-Kolchin, M., Bullock, J. S., & Kaplinghat, M. 2012, MNRAS, 422, 1203

Bregman, J. N., & Lloyd-Davies, E. J. 2007, ApJ, 669, 990

Bregman, J. N., Snider, B. A., Grego, L., & Cox, C. V. 1998, ApJ, 499, 670

Bullock, J. S., Dekel, A., Kolatt, T. S., Primack, J. R., & Somerville, R. S. 2001, ApJ, 550, 21

Cen, R., & Ostriker, J. P. 2006, ApJ, 650, 560

Crain, R. A., McCarthy, I. G., Frenk, C. S., Theuns, T., & Schaye, J. 2010, MNRAS, 407, 1403

Crawford, F., Kaspi, V. M., Manchester, R. N., et al. 2001, ApJ, 553, 367

Dai, X., Bregman, J. N., Kochanek, C. S., & Rasia, E. 2010, ApJ, 719, 119

de Boer, K. S., Braun, J. M., Vallenari, A., & Mebold, U. 1998, A&A, 329, L49

Dekel, A., & Birnboim, Y. 2006, MNRAS, 368, 2

Dekel, A., & Silk, J. 1986, ApJ, 303, 39

Fang, T., Mckee, C. F., Canizares, C. R., & Wolfire, M. 2006, ApJ, 644, 174

Fang, T., Sembach, K. R., & Canizares, C. R. 2003, ApJ, 586, L49

Fox, A. J., Wakker, B. P., Savage, B. D., et al. 2005, ApJ, 630, 332

Fox, A. J., Wakker, B. P., Smoker, J. V., et al. 2010, ApJ, 718, 1046

Fukugita, M., Hogan, C. J., & Peebles, P. J. E. 1998, ApJ, 503, 518

Fukugita, M., & Peebles, P. J. E. 2006, ApJ, 639, 590

Gaensler, B. M., Madsen, G. J., Chatterjee, S., & Mao, S. A. 2008, Publications of the Astronomical Society of Australia, 25, 184

Grcevich, J., & Putman, M. E. 2009, ApJ, 696, 385

Gupta, A., Mathur, S., Krongold, Y., Nicastro, F., & Galeazzi, M. 2012, ArXiv e-prints

Hagihara, T., Yao, Y., Yamasaki, N. Y., et al. 2010, PASJ, 62, 723

Henley, D. B., & Shelton, R. L. 2010, ApJS, 187, 388

Humphrey, P. J., Buote, D. A., Canizares, C. R., Fabian, A. C., & Miller, J. M. 2011, ApJ, 729, 53

Kalberla, P. M. W., & Kerp, J. 2009, ARA&A, 47, 27

Kaufmann, T., Bullock, J. S., Maller, A. H., Fang, T., & Wadsley, J. 2009, MNRAS, 396, 191

Kereš, D., & Hernquist, L. 2009, ApJ, 700, L1

Kereš, D., Katz, N., Weinberg, D. H., & Davé, R. 2005, MNRAS, 363, 2

Komatsu, E., Smith, K. M., Dunkley, J., et al. 2011, ApJS, 192, 18

Kuntz, K. D., & Snowden, S. L. 2000, ApJ, 543, 195

Li, Y., Mo, H. J., van den Bosch, F. C., & Lin, W. P. 2007, MNRAS, 379, 689

Lin, D. N. C., & Faber, S. M. 1983, ApJ, 266, L21

Maller, A. H., & Bullock, J. S. 2004, MNRAS, 355, 694

Manchester, R. N., Fan, G., Lyne, A. G., Kaspi, V. M., & Crawford, F. 2006, ApJ, 649, 235

McConnachie, A. W. 2012, AJ, 144, 4

McLaughlin, M. A., & Cordes, J. M. 2003, ApJ, 596, 982

McMillan, P. J., & Binney, J. 2012, MNRAS, 419, 2251

Mo, H. J., & Mao, S. 2002, MNRAS, 333, 768

Mo, H. J., & Miralda-Escude, J. 1996, ApJ, 469, 589

Mo, H. J., Yang, X., van den Bosch, F. C., & Katz, N. 2005, MNRAS, 363, 1155

Moore, B., & Davis, M. 1994, MNRAS, 270, 209

Moster, B. P., Naab, T., & White, S. D. M. 2012, ArXiv e-prints

Navarro, J. F., Frenk, C. S., & White, S. D. M. 1997, ApJ, 490, 493

Nicastro, F., Zezas, A., Drake, J., et al. 2002, ApJ, 573, 157

Nichols, M., Colless, J., Colless, M., & Bland-Hawthorn, J. 2011, ApJ, 742, 110

Prochaska, J. X., Kasen, D., & Rubin, K. 2011, ApJ, 734, 24

Putman, M. E., Saul, D. R., & Mets, E. 2011, MNRAS, 418, 1575

Rasmussen, J., & Ponman, T. J. 2009, MNRAS, 399, 239

Rasmussen, J., Sommer-Larsen, J., Pedersen, K., et al. 2009, ApJ, 697, 79

Reynolds, R. J. 1989, ApJ, 339, L29

Sharma, P., McCourt, M., Quataert, E., & Parrish, I. J. 2012, MNRAS, 420, 3174

Silk, J. 1977, ApJ, 211, 638

Sommer-Larsen, J. 2006, ApJ, 644, L1

Spitzer, Jr., L. 1956, ApJ, 124, 20

Stanimirović, S., Dickey, J. M., Krčo, M., & Brooks, A. M. 2002, ApJ, 576, 773

Sternberg, A., McKee, C. F., & Wolfire, M. G. 2002, ApJS, 143, 419

Sutherland, R. S., & Dopita, M. A. 1993, ApJS, 88, 253

Wang, Q. D. 2007, in EAS Publications Series, Vol. 24, EAS Publications Series, ed. E. Emsellem, H. Wozniak, G. Massacrier, J.-F. Gonzalez, J. Devriendt, & N. Champavert, 59–72

Weiner, B. J., & Williams, T. B. 1996, AJ, 111, 1156

White, S. D. M., & Frenk, C. S. 1991, ApJ, 379, 52

White, S. D. M., & Rees, M. J. 1978, MNRAS, 183, 341

Yao, Y., Tripp, T. M., Wang, Q. D., et al. 2009a, ApJ, 697, 1784

Yao, Y., Wang, Q. D., Hagihara, T., et al. 2009b, ApJ, 690, 143

Yoshino, T., Mitsuda, K., Yamasaki, N. Y., et al. 2009, PASJ, 61, 805